

MPAS

Model for Prediction Across Scales

Bill Skamarock, Joe Klemp, Michael Duda,
Laura Fowler, Sang-Hun Park
National Center for Atmospheric Research

Based on unstructured centroidal Voronoi (hexagonal) meshes using C-grid staggering and selective grid refinement.

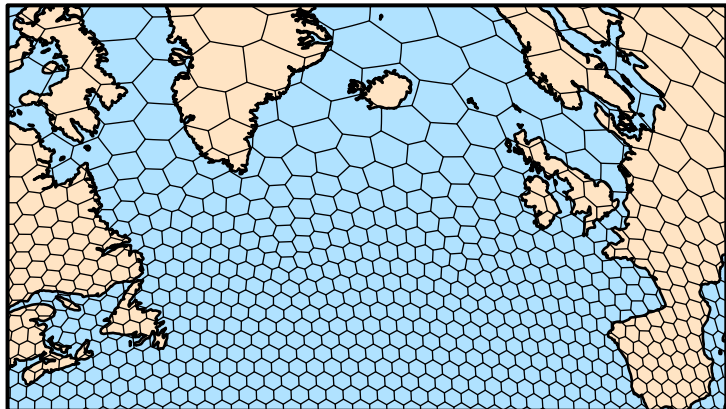
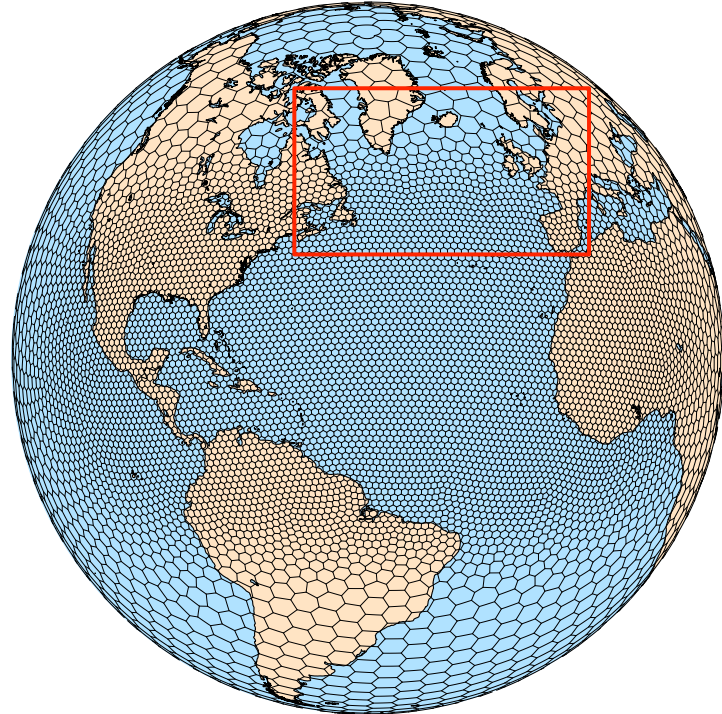
Collaboratively developed, primarily by NCAR and LANL/DOE

MPAS infrastructure - NCAR, LANL, others.

MPAS - Atmosphere (NCAR)

MPAS - Ocean (LANL)

MPAS - Ice, etc. (LANL and others)



U.S. DEPARTMENT OF
ENERGY

Office of
Science



MPAS Nonhydrostatic Atmospheric Solver

Fully Compressible Nonhydrostatic Equations

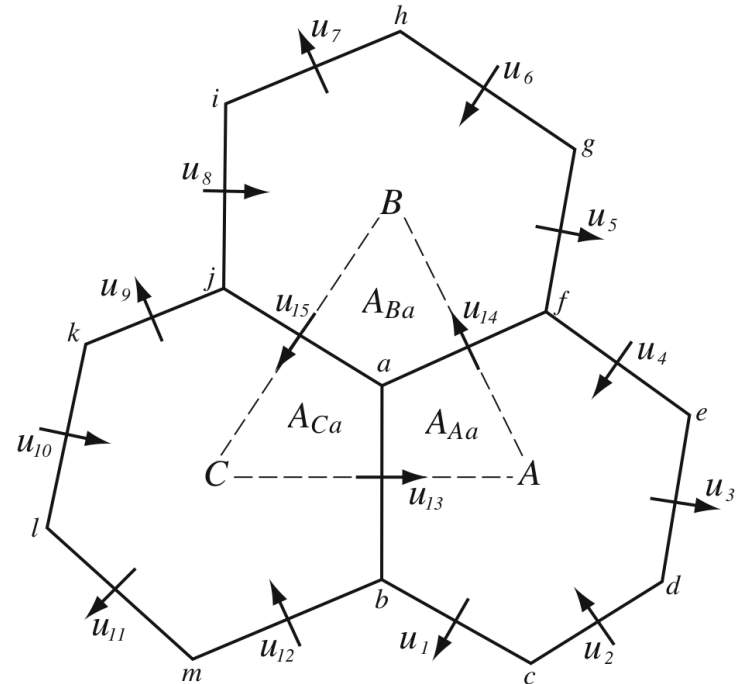
- Prognostic equations for coupled variables.
- Generalized height coordinate.
- Horizontally vector invariant eqn set.
- Continuity equation for dry air mass.
- Thermodynamic equation for coupled potential temperature.

Time integration as in Advanced Research WRF

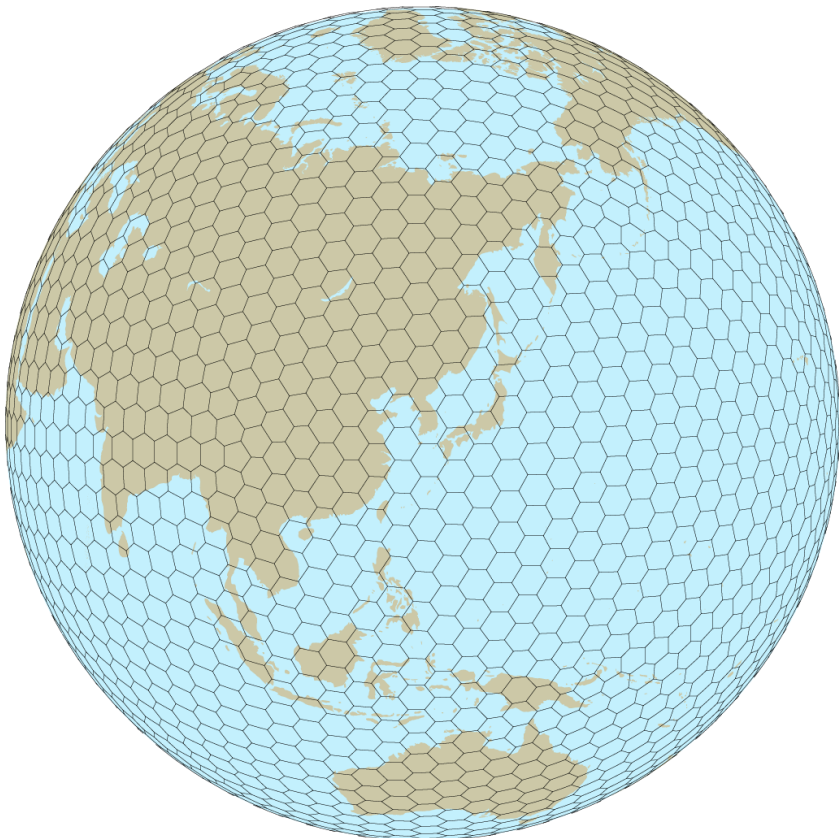
- Split-explicit Runge-Kutta (3rd order)

Full complement of atmospheric-model physics

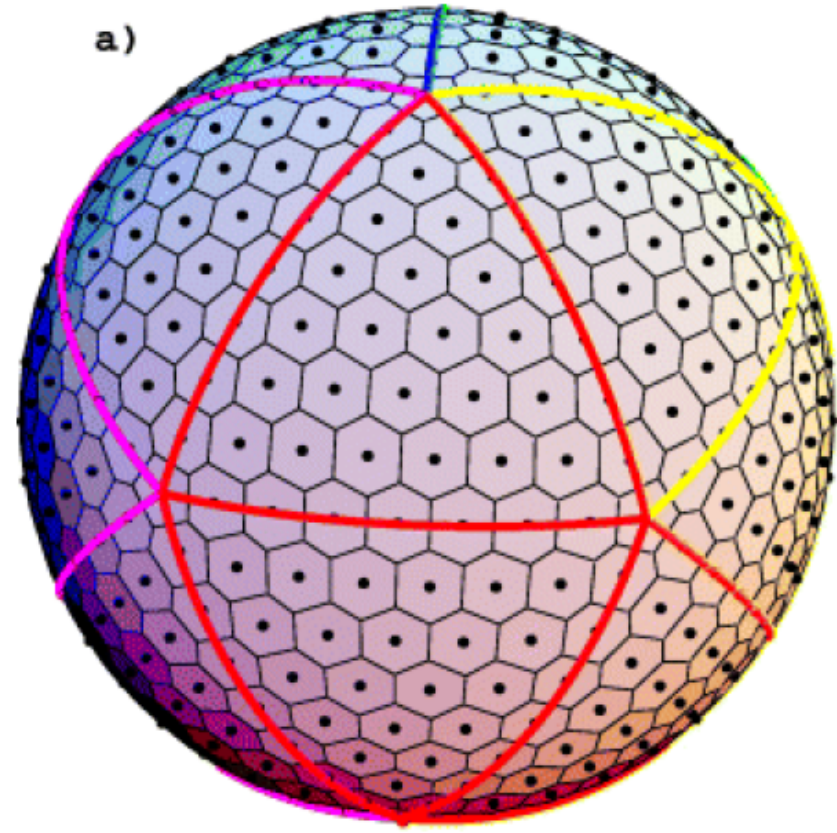
MPAS is based on unstructured centroidal Voronoi (hexagonal) meshes using C-grid staggering and selective grid refinement.



Global Meshes



Global Quasi-Uniform Mesh
(SCVT)

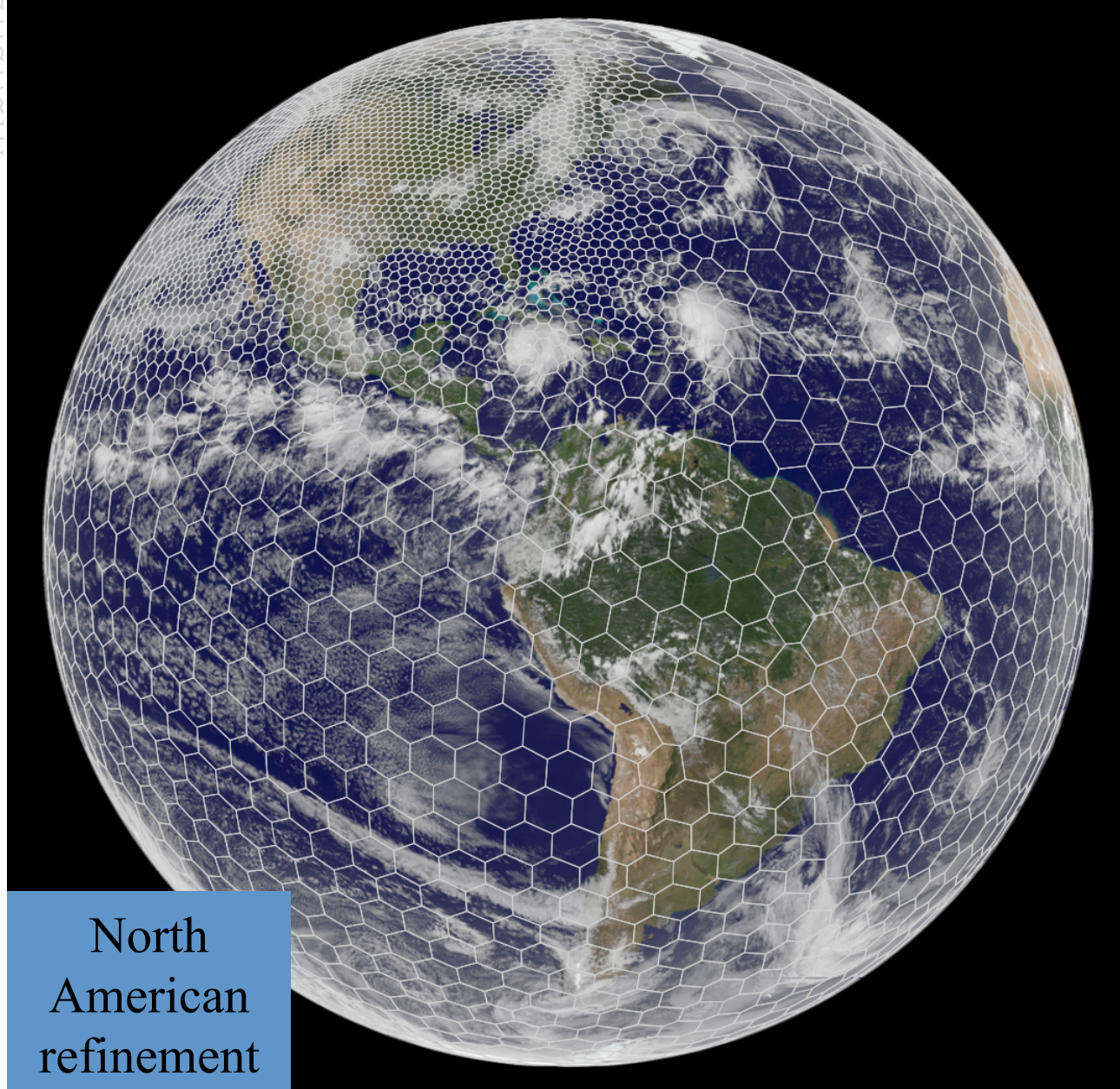


Many models use an icsoahedral mesh
(NICAM, BUGS, FIM, NIM, OLAM, etc.)

Mesh generation

Lloyd's method
(iterative)
using a user-supplied
density function

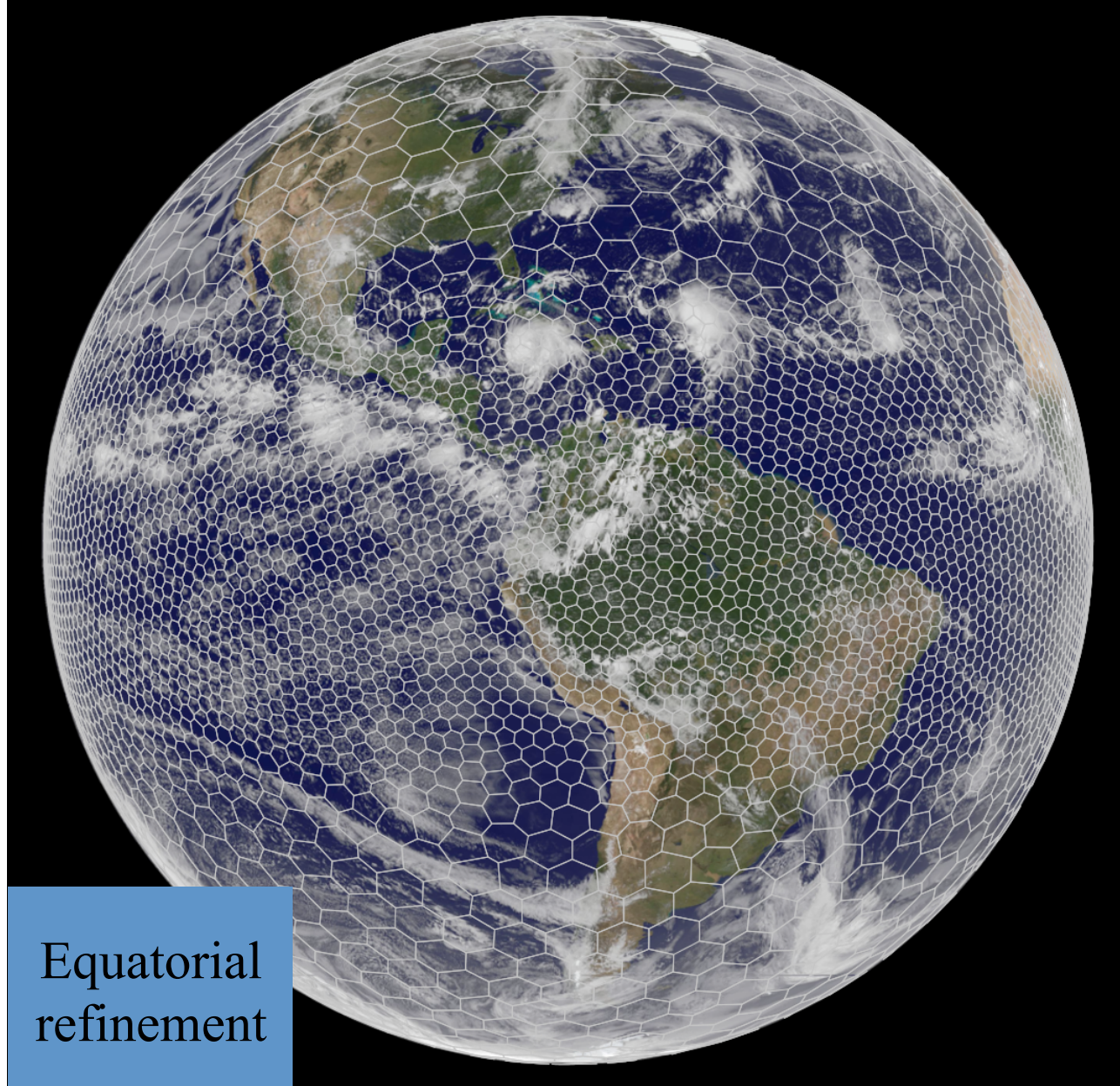
North
American
refinement



Mesh generation

Lloyd's method
(iterative)
using a user-supplied
density function

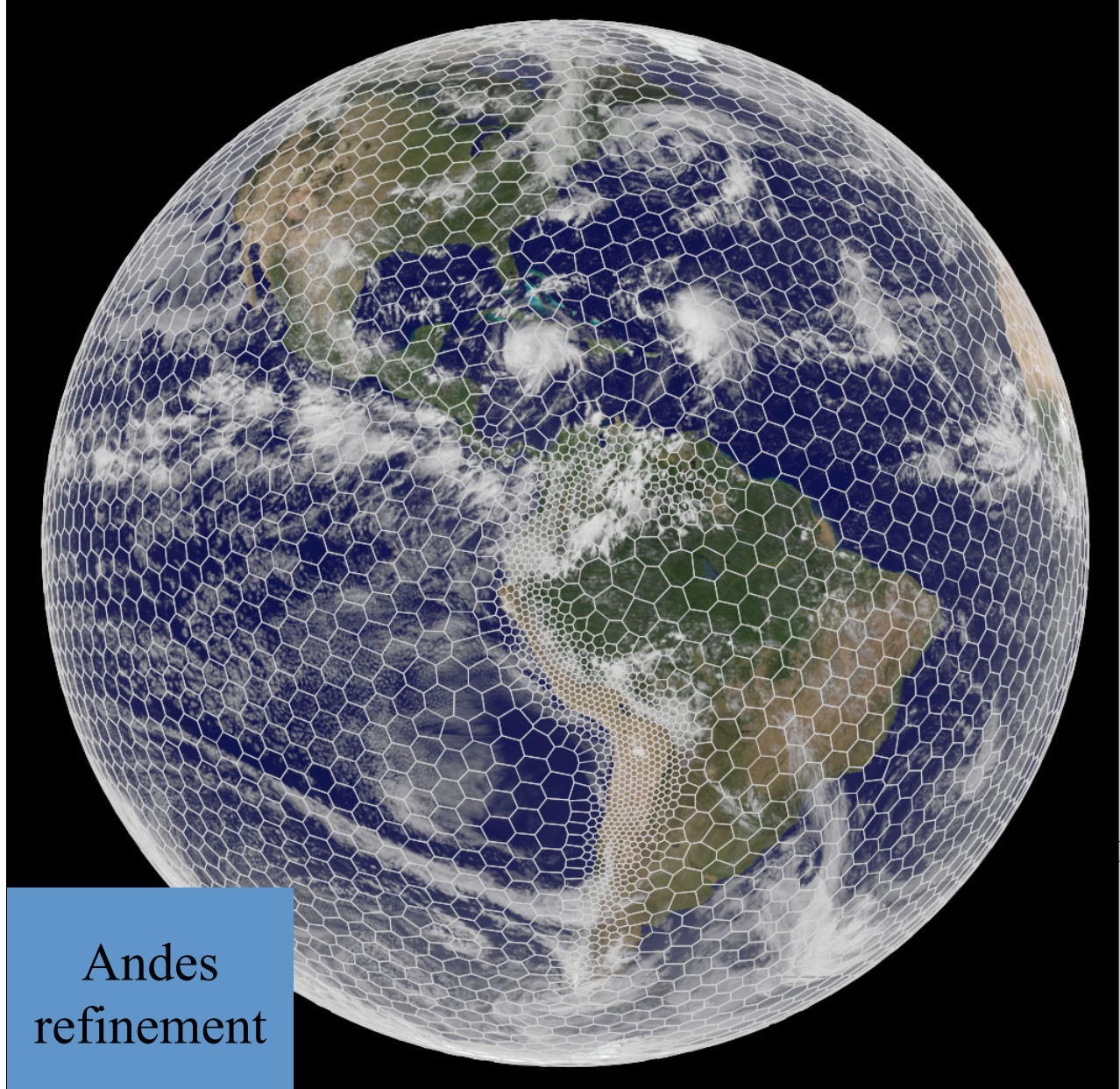
Equatorial
refinement



Mesh generation

Lloyd's method
(iterative)
using a user-supplied
density function

Andes
refinement



MPAS Nonhydrostatic Atmospheric Solver

Prognostic
equations:

$$\begin{aligned} \frac{\partial \mathbf{V}_H}{\partial t} = & - \frac{\rho_d}{\rho_m} \left[\nabla_\zeta \left(\frac{p}{\zeta_z} \right) - \frac{\partial \mathbf{z}_{HP}}{\partial \zeta} \right] - \eta \mathbf{k} \times \mathbf{v}_H \\ & - \mathbf{v}_H \nabla_\zeta \cdot \mathbf{V} - \frac{\partial \Omega \mathbf{v}_H}{\partial \zeta} - \rho_d \nabla_\zeta K - \beta_d \left(eW \cos \alpha_r + \frac{uW}{r} \right) + \mathbf{F}_{V_H}, \\ \frac{\partial W}{\partial t} = & - \frac{\rho_d}{\rho_m} \left[\frac{\partial p}{\partial \zeta} + g \tilde{\rho}_m \right] - (\nabla \cdot \mathbf{v} W)_\zeta \\ & + \beta_d \left[\frac{uU + vV}{r} + e(U \cos \alpha_r - V \sin \alpha_r) \right] + F_W, \\ \frac{\partial \Theta_m}{\partial t} = & - (\nabla \cdot \mathbf{V} \theta_m)_\zeta + F_{\Theta_m}, \\ \frac{\partial \rho_d}{\partial t} = & - (\nabla \cdot \mathbf{V})_\zeta, \\ \frac{\partial Q_j}{\partial t} = & - (\nabla \cdot \mathbf{V} q_j)_\zeta + F_{Q_j}. \end{aligned}$$

(1) Gradient operators

(2) Flux divergence operators

(3) Nonlinear Coriolis term

$\beta_d = 0, r = r_{\text{earth}}$: shallow atmosphere approximation

Operators on the Voronoi Mesh

Flux divergence and transport

Transport equation, conservative form:

$$\frac{\partial(\rho\psi)}{\partial t} = -\nabla \cdot \mathbf{V}(\rho\psi)$$

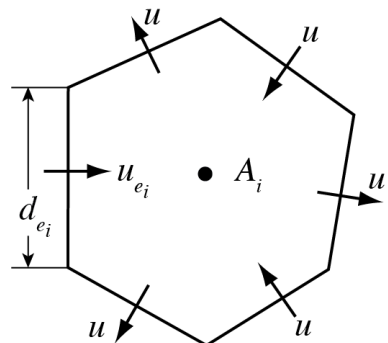
Finite-Volume formulation,
Integrate over cell:

$$\int_D \left[\frac{\partial}{\partial t}(\rho\psi) = -\nabla \cdot \mathbf{V}(\rho\psi) \right] dV$$

Apply divergence theorem:

$$\frac{\partial(\overline{\rho\psi})}{\partial t} = -\frac{1}{V} \int_{\Sigma} (\rho\psi) \mathbf{V} \cdot \mathbf{n} d\sigma$$

Discretize in time and space: $(\rho\psi)_i^{t+\Delta t} = (\rho\psi)_i^t - \Delta t \frac{1}{A_i} \sum_{n_{e_i}} d_{e_i} \overline{(\rho \mathbf{V} \cdot \mathbf{n}_{e_i}) \psi}$



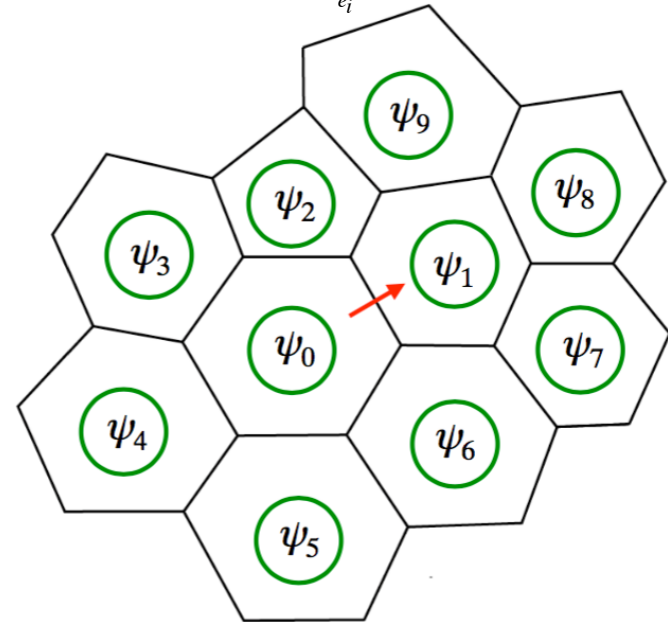
Velocity divergence operator is 2nd-order accurate for edge-centered velocities.

Flux divergence, transport, and Runge-Kutta time integration

Scalar transport equation for cell i :

$$\frac{\partial(\rho\psi)_i}{\partial t} = L(\mathbf{V}, \rho, \psi) = -\frac{1}{A_i} \sum_{n_{e_i}} d_{e_i} (\rho \mathbf{V} \cdot \bar{n}_{e_i}) \bar{\psi}$$

1. Scalar edge-flux value y is the weighted sum of cell values from cells that share edge and all their neighbors.
2. An individual edge-flux is used to update the two cells that share the edge.
3. Three edge-flux evaluations and cell updates are needed to complete the Runge-Kutta timestep.
4. Monotonic constraint requires checking the cell-value update and renormalizing edge-fluxes if the cell updates are outside specific bounds (on the final RK3 update).



$$(\rho\psi)^* = (\rho\psi)^t + \frac{\Delta t}{3} L(\mathbf{V}, \rho, \psi^t)$$

$$(\rho\psi)^{**} = (\rho\psi)^t + \frac{\Delta t}{2} L(\mathbf{V}, \rho, \psi^*)$$

$$(\rho\psi)^{t+\Delta t} = (\rho\psi)^t + \Delta t L(\mathbf{V}, \rho, \psi^{**})$$

Operators on the Voronoi Mesh

Flux divergence and transport

3rd and 4th-order fluxes (e.g. in WRF):

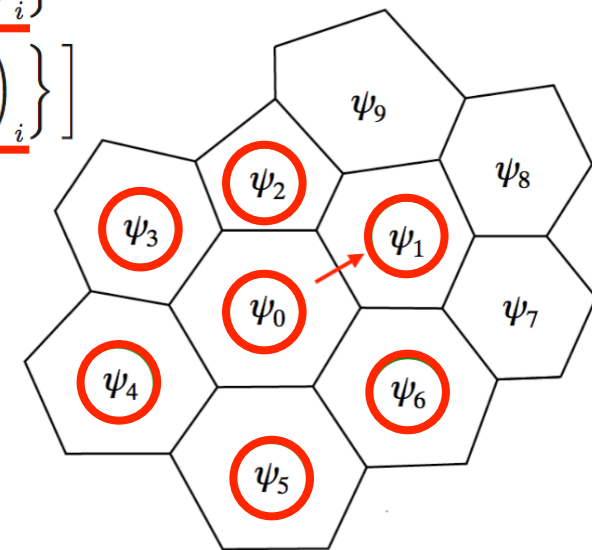
$$F(u, \psi)_{i+1/2} = u_{i+1/2} \left[\frac{1}{2} (\psi_{i+1} + \psi_i) - \frac{1}{12} (\delta_x^2 \psi_{i+1} + \delta_x^2 \psi_i) + \text{sign}(u) \frac{\beta}{12} (\delta_x^2 \psi_{i+1} - \delta_x^2 \psi_i) \right]$$

where $\delta_x^2 \psi_i = \psi_{i-1} - 2\psi_i + \psi_{i+1}$ (Hundsdorfer et al, 1995; Van Leer, 1985)

Recognizing $\delta_x^2 \psi = \Delta x^2 \frac{\partial^2 \psi}{\partial x^2} + O(\Delta x^4)$ we recast the 3rd and 4th order flux as

$$\begin{aligned} F(u, \psi)_{i+1/2} = u_{i+1/2} & \left[\frac{1}{2} (\psi_{i+1} + \psi_i) - \Delta x_e^2 \frac{1}{12} \left\{ \left(\frac{\partial^2 \psi}{\partial x^2} \right)_{i+1} + \underbrace{\left(\frac{\partial^2 \psi}{\partial x^2} \right)_i}_{\text{red}} \right\} \right. \\ & \left. + \text{sign}(u) \Delta x_e^2 \frac{\beta}{12} \left\{ \left(\frac{\partial^2 \psi}{\partial x^2} \right)_{i+1} - \underbrace{\left(\frac{\partial^2 \psi}{\partial x^2} \right)_i}_{\text{red}} \right\} \right] \end{aligned}$$

where x is the direction normal to the cell edge and i and $i+1$ are cell centers. We use the least-squares-fit polynomial to compute the second derivatives.



Operators on the Voronoi Mesh

Flux divergence and transport

3rd and 4th-order fluxes (e.g. in WRF):

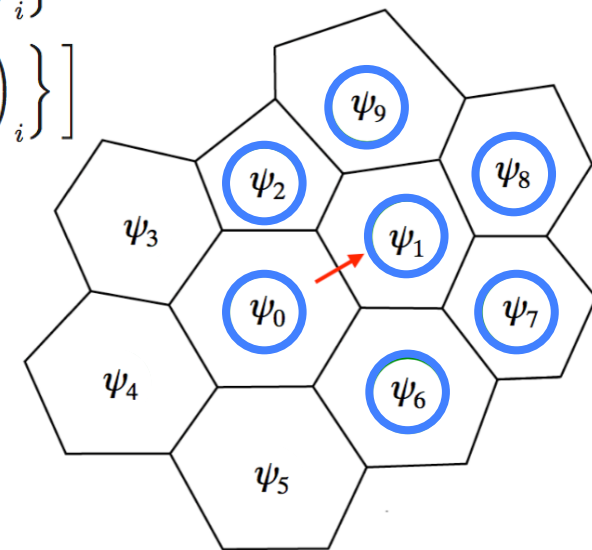
$$F(u, \psi)_{i+1/2} = u_{i+1/2} \left[\frac{1}{2} (\psi_{i+1} + \psi_i) - \frac{1}{12} (\delta_x^2 \psi_{i+1} + \delta_x^2 \psi_i) + \text{sign}(u) \frac{\beta}{12} (\delta_x^2 \psi_{i+1} - \delta_x^2 \psi_i) \right]$$

where $\delta_x^2 \psi_i = \psi_{i-1} - 2\psi_i + \psi_{i+1}$ (Hundsdorfer et al, 1995; Van Leer, 1985)

Recognizing $\delta_x^2 \psi = \Delta x^2 \frac{\partial^2 \psi}{\partial x^2} + O(\Delta x^4)$ we recast the 3rd and 4th order flux as

$$\begin{aligned} F(u, \psi)_{i+1/2} = u_{i+1/2} & \left[\frac{1}{2} (\psi_{i+1} + \psi_i) - \Delta x_e^2 \frac{1}{12} \left\{ \underbrace{\left(\frac{\partial^2 \psi}{\partial x^2} \right)_{i+1}}_{\text{second derivative at } i+1} + \left(\frac{\partial^2 \psi}{\partial x^2} \right)_i \right\} \right. \\ & \left. + \text{sign}(u) \Delta x_e^2 \frac{\beta}{12} \left\{ \underbrace{\left(\frac{\partial^2 \psi}{\partial x^2} \right)_{i+1}}_{\text{second derivative at } i+1} - \left(\frac{\partial^2 \psi}{\partial x^2} \right)_i \right\} \right] \end{aligned}$$

where x is the direction normal to the cell edge and i and $i+1$ are cell centers. We use the least-squares-fit polynomial to compute the second derivatives.



Operators on the Voronoi Mesh 'Nonlinear' Coriolis force

$$\frac{\partial \mathbf{V}_H}{\partial t} = -\frac{\rho_d}{\rho_m} \left[\nabla_\zeta \left(\frac{p}{\zeta_z} \right) - \frac{\partial \mathbf{z}_H p}{\partial \zeta} \right] - \eta \mathbf{k} \times \mathbf{V}_H \\ - \mathbf{v}_H \nabla_\zeta \cdot \mathbf{V} - \frac{\partial \Omega \mathbf{v}_H}{\partial \zeta} - \rho_d \nabla_\zeta K - \beta_d \left(eW \cos \alpha_r + \frac{uW}{r} \right) + \mathbf{F}_{V_H}$$

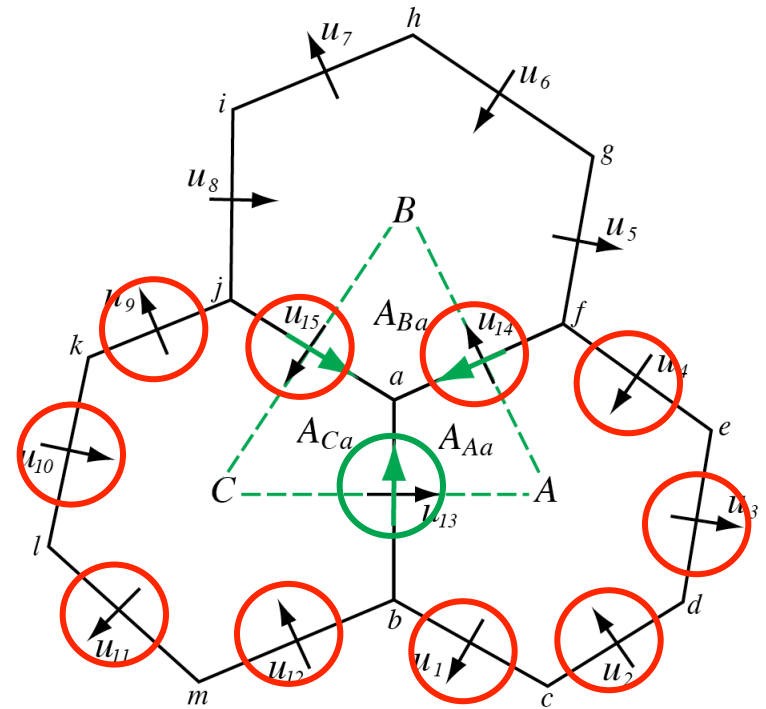
Tangential velocity

reconstruction: $v_{e_i} = \sum_{j=1}^{n_{e_i}} w_{e_i,j} u_{e_i,j}$

Nonlinear term:

$$[\eta \mathbf{k} \times \mathbf{V}_H]_{e_i} = \sum_{j=1}^{n_{e_i}} \frac{1}{2} (\eta_{e_i} + \eta_{e_i,j}) w_{e_i,j} \rho_{e_i,j} u_{e_i,j}$$

The general tangential velocity reconstruction produces a consistent divergence on the primal and dual grids, and allows for PV, enstrophy and energy* conservation in the nonlinear SW solver.



Operators on the Voronoi Mesh

'Nonlinear' Coriolis force

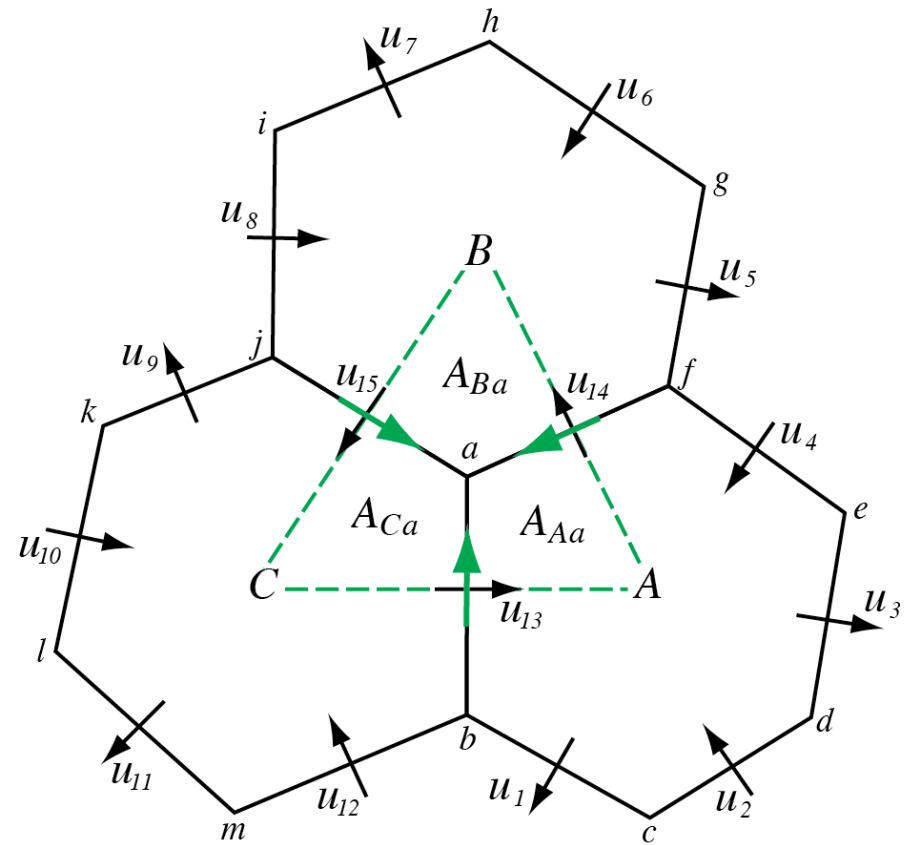
$$[\eta \mathbf{k} \times \mathbf{V}_H]_{e_i} = \sum_{j=1}^{n_{e_i}} \frac{1}{2} (\eta_{e_i} + \eta_{e_{i,j}}) w_{e_{i,j}} \rho_{e_{i,j}} u_{e_{i,j}}$$

Example: absolute vorticity at e_{13}

$$\eta_{13} = \frac{1}{2} (\eta_a + \eta_b)$$

Example: absolute vorticity at vertex a

$$\eta_a = f_a + \frac{\left(u_{13} |\overrightarrow{CA}| + u_{14} |\overrightarrow{AB}| + u_{15} |\overrightarrow{BC}| \right)}{\text{Area}(ABC)}$$



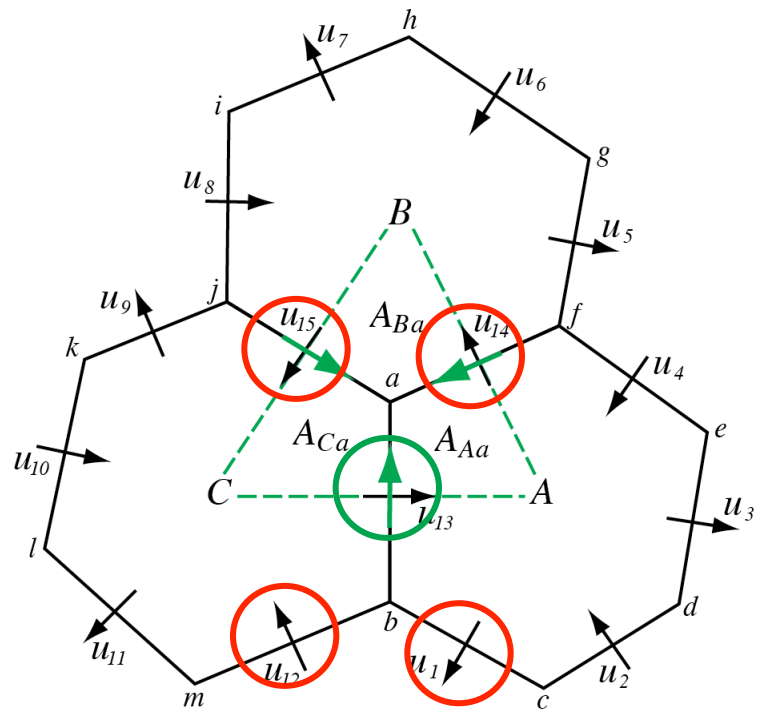
Operators in MPAS – ‘nonlinear Coriolis force’

Why do we use so many velocities to reconstruct the tangential velocity?

Consider constructing tangential velocities from weighted sum of the four nearest neighbors.

Result: physically stationary geostrophic modes (geostrophically-balanced flow) will not be stationary in the discrete system; the solver is unusable.

(Nickovic et al, MWR 2002)



Operators in MPAS – ‘nonlinear Coriolis force’

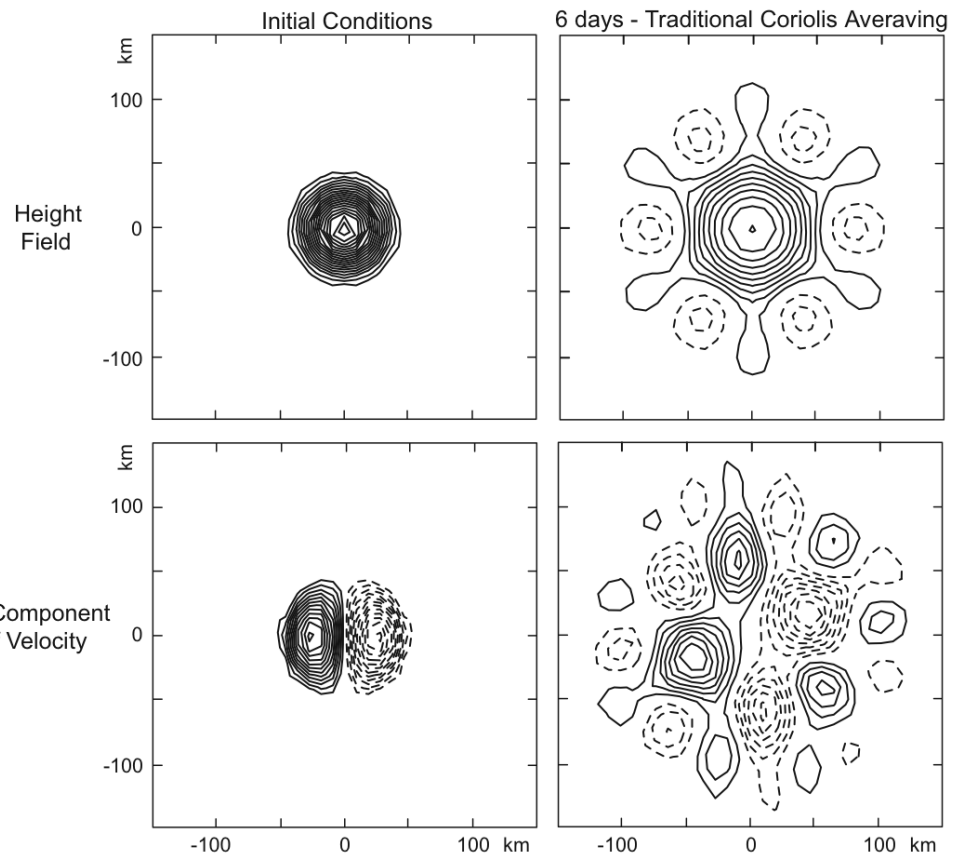
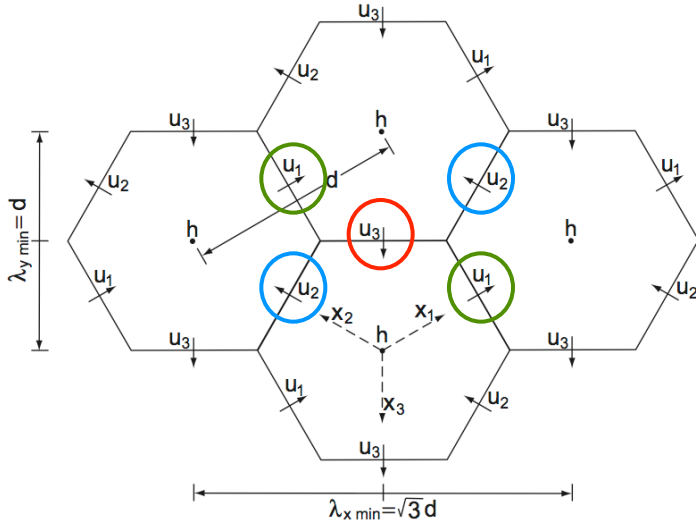
Traditional Coriolis velocity evaluation

$$\partial_t u_1 + g \delta_{x_1} h + \frac{f}{\sqrt{3}} (u_{31} - u_{21}) = 0$$

$$\partial_t u_2 + g \delta_{x_2} h + \frac{f}{\sqrt{3}} (u_{12} - u_{32}) = 0$$

$$\partial_t u_3 + g \delta_{x_3} h + \frac{f}{\sqrt{3}} (u_{23} + u_{13}) = 0$$

$$\partial_t h + \frac{2}{3} H (\delta_{x_1} u_1 + \delta_{x_2} u_2 + \delta_{x_3} u_3) = 0$$



Operators in MPAS – ‘nonlinear Coriolis force’

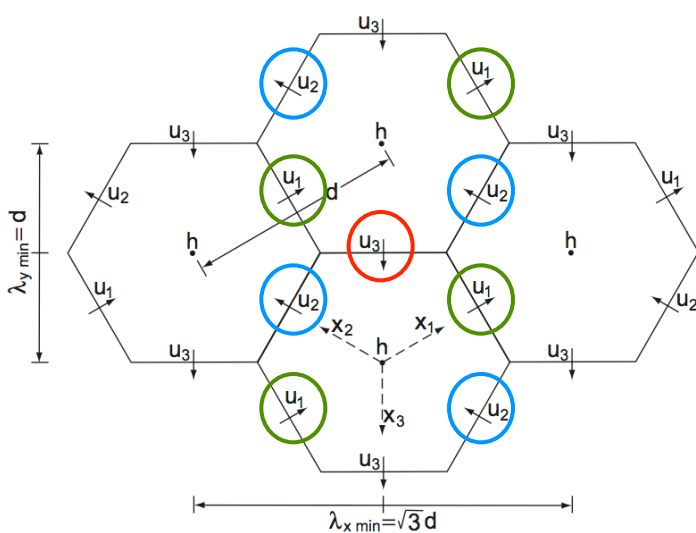
New Coriolis velocity evaluation (Thuburn et al, 2009 JCP)

$$\partial_t u_1 + g \delta_{x_1} h + \frac{f}{\sqrt{3}} (u_{31} - u_{21}) = 0$$

$$\partial_t u_2 + g \delta_{x_2} h + \frac{f}{\sqrt{3}} (u_{12} - u_{32}) = 0$$

$$\partial_t u_3 + g \delta_{x_3} h + \frac{f}{\sqrt{3}} (u_{23} + u_{13}) = 0$$

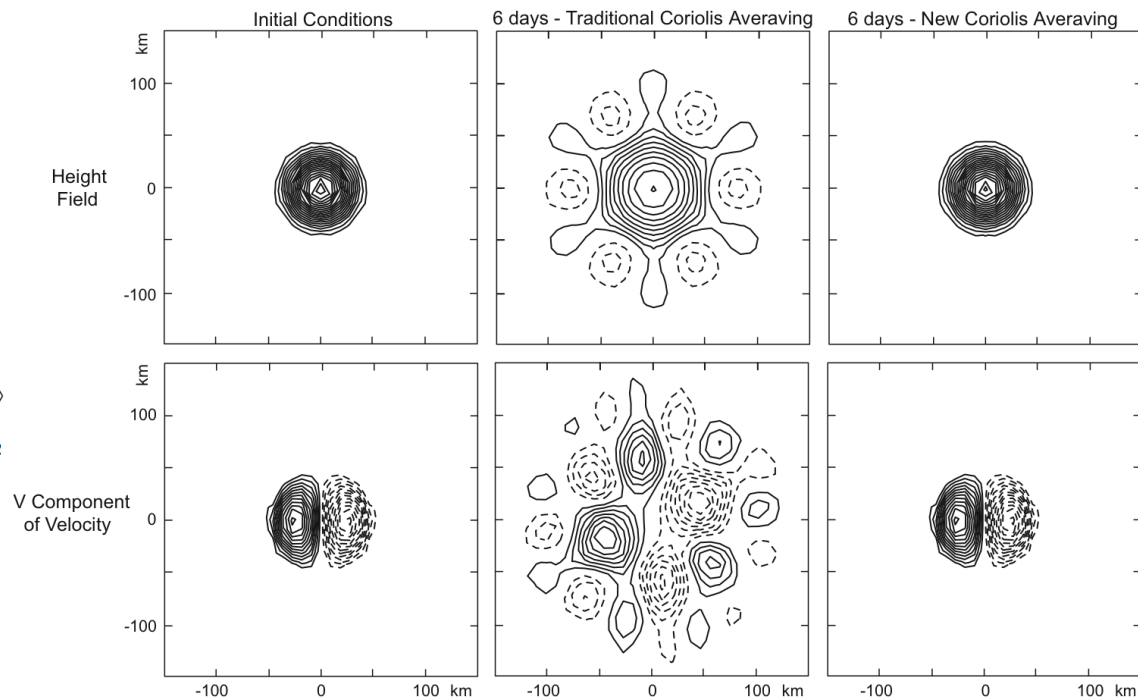
$$\partial_t h + \frac{2}{3} H (\delta_{x_1} u_1 + \delta_{x_2} u_2 + \delta_{x_3} u_3) = 0$$



$$u_{21} = \frac{1}{3} \overline{u_2}^{x_3} + \frac{2}{3} \overline{\overline{u_2}}^{x_1} x_2, \quad u_{31} = \frac{1}{3} \overline{u_3}^{x_2} + \frac{2}{3} \overline{\overline{u_3}}^{x_1} x_3,$$

$$u_{12} = \frac{1}{3} \overline{u_1}^{x_3} + \frac{2}{3} \overline{\overline{u_1}}^{x_1} x_2, \quad u_{32} = \frac{1}{3} \overline{u_3}^{x_1} + \frac{2}{3} \overline{\overline{u_3}}^{x_2} x_3,$$

$$u_{13} = \frac{1}{3} \overline{u_1}^{x_2} + \frac{2}{3} \overline{\overline{u_1}}^{x_1} x_3, \quad u_{23} = \frac{1}{3} \overline{u_2}^{x_1} + \frac{2}{3} \overline{\overline{u_2}}^{x_2} x_3$$



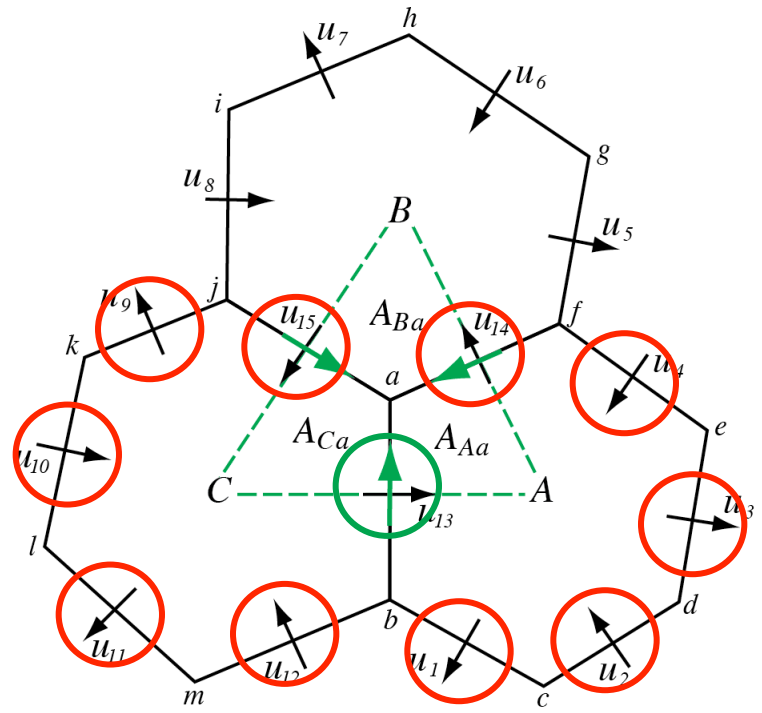
Operators in MPAS – ‘nonlinear Coriolis force’

$$\begin{aligned}\frac{\partial \mathbf{V}_H}{\partial t} = & -\frac{\rho_d}{\rho_m} \left[\nabla_\zeta \left(\frac{p}{\zeta_z} \right) - \frac{\partial \mathbf{z}_H p}{\partial \zeta} \right] - \eta \mathbf{k} \times \mathbf{V}_H \\ & - \mathbf{v}_H \nabla_\zeta \cdot \mathbf{V} - \frac{\partial \Omega \mathbf{v}_H}{\partial \zeta} - \rho_d \nabla_\zeta K - \beta_d \left(eW \cos \alpha_r + \frac{uW}{r} \right) + \mathbf{F}_{V_H}\end{aligned}$$

Results: stationary geostrophic modes are stationary; local and global mass and PV conservation is obtained on the dual (triangular) mesh (for the SW equations).

$$\begin{aligned}\mathbf{k} \cdot \nabla \times \left[\frac{\partial \mathbf{u}}{\partial t} + q(h \mathbf{u}^\perp) \right] &= -g \nabla (h + h_s) - \nabla K \\ \frac{\partial(hq)}{\partial t} + \nabla \cdot [hq \mathbf{u}^\perp] &= 0\end{aligned}$$

potential vorticity flux



MPAS Solver (and Physics) Information

<http://mpas-dev.github.io/>



[MPAS Home](#)

Overview

[MPAS-Atmosphere](#)

[MPAS-Land Ice](#)

[MPAS-Ocean](#)

[Data Assimilation](#)

[Publications](#)

[Presentations](#)

Download

[MPAS-Atmosphere download](#)

[MPAS-Land Ice download](#)

[MPAS-Ocean download](#)

Resources

[License Information](#)

[Wiki](#)

[Bug Tracker](#)

[Mailing Lists](#)

[MPAS Developers Guide](#)

Error Characteristics of Two Grid Refinement Approaches in Aquaplanet Simulations: MPAS-A and WRF. Hagos, S., Leung, R., Rauscher, S. A., & Ringler, T., 2013, 141(9), 3022–3036. doi:10.1175/MWR-D-12-00338.1 ([pdf](#))

2012

Exploring a Global Multi-Resolution Modeling Approach Using Aquaplanet Simulations. S. Rauscher, T. Ringler, W. Skamarock, and A. Mirin, 2012, J. Climate., 26, 2432-2452, doi:10.1175/JCLI-D-12- 00154.1 [pdf](#)



A Multi-scale Nonhydrostatic Atmospheric Model Using Centroidal Voronoi Tesselations and C-Grid Staggering. William C. Skamarock, Joseph B. Klemp, Michael G. Duda, Laura Fowler, Sang-Hun Park, and Todd D. Ringler. 2012 Monthly Weather Review, 240, 3090-3105, doi:10.1175/MWR-D-11-00215.1 [pdf](#)

2011

A Terrain-Following Coordinate with Smoothed Coordinate Surfaces. Joseph B. Klemp, 2011, Monthly Weather Review, 139(7), 2163–2169. [doi:10.1175/MWR-D-10-05046.1](#)

Conservative Transport Schemes for Spherical Geodesic Grids: High-Order Flux Operators for ODE-Based Time Integration. W. Skamarock and A. Gassmann, 2011, Monthly Weather Review, Vol. 139, pp. 2962-2975, doi:10.1175/MWR-D-10-05056.1 [pdf](#)

Exploring a Multi-Resolution Modeling Approach within the Shallow-Water Equations. Ringler, T., D.W. Jacobsen, M. Gunzburger, L. Ju, M. Duda and W. Skamarock, 2011, Monthly Weather Review, DOI: [10.1175/MWR-D-10-05046.1](#)